Chapter 4
Modeling of Stochastic Ca^{2+} Signals

Sten Rüdiger and Jianwei Shuai

Abstract It has been shown that IP_3R channels are distributed in clusters on the membrane of the endoplasmic reticulum, generating Ca^{2+} signals on multiple scales, from local puffs to global intra- and intercellular waves. Local Ca^{2+} puffs released from a cluster of IP_3R s are strongly stochastic. The most obvious source of noise for puffs is the small number of channels within a cluster. In this chapter we discuss the simulation of stochastic Ca^{2+} signals. Various simulation methods such as the Gillespie algorithm, a two-state Markovian chain, and gate-based and channel-based Langevin approaches have been introduced for use in the study of stochastic gating dynamics of IP_3R channels. Combining the stochastic channel dynamics with the deterministic simulation the Ca^{2+} diffusion process, the fluctuating Ca^{2+} signals, including puffs and both intra- and intercellular waves, can be investigated by hybrid models.

Keywords Stochastic processes · Calcium signaling · Channel gating dynamics Inositol 1,4,5-trisphosphate receptor · Calcium puffs · Calcium sparks · Calcium waves · Intracellular waves · Intercellular waves

4.1 Introduction

Calcium is a ubiquitous mediator of cellular responses to external stimuli including neurotransmitters, hormones and mechanical stresses. The stimulus is represented by transient or repetitive increases of cytosolic Ca^{2+} concentrations. In astrocytes, for example, oscillations of $[Ca^{2+}]$ enable intercellular communication and are linked to the plasticity of neuronal synapses (Volterra et al. 2014; Rusakov 2015). Ca^{2+} was shown to regulate gene expression by involving a number of transcription factors

S. Rüdiger (✉)
Institute of Physics, Humboldt-Universität zu Berlin, Berlin, Germany
e-mail: sten.ruediger@physik.hu-berlin.de

J. Shuai
Department of Physics and State Key Laboratory of Cellular Stress Biology, Innovation Center for Cell Signaling Network, Xiamen University, Xiamen 361005, China
e-mail: jianweishuai@xmu.edu.cn

M. De Pittà and H. Berry (eds.), *Computational Glioscience*, Springer Series in Computational Neuroscience, https://doi.org/10.1007/978-3-030-00817-8_4

(Dolmetsch et al. 1998; Di Capite et al. 2009). The regulation of a multitude of such processes emerges from the tuning of Ca^{2+} levels in space and time.

Cytosolic Ca^{2+} levels are structured by coordinated release from intracellular stores located in cell organelles, particularly the endoplasmic reticulum (ER). The release from stores occurs through two related types of receptor channels in the membrane of the ER: inositol trisphosphate receptors (IP_3Rs) and ryanodine receptors (RyRs). The receptor channels regulate Ca^{2+} release in response to the binding of specific ligands, including Ca^{2+}, to binding sites on the cytosolic side of the channels. Ca^{2+} released by a channel diffuses into the cytosol and increases the probability of neighboring channels being open by binding to their activating binding sites. This provides a self-amplifying mechanism called Ca^{2+}-induced Ca^{2+} release (CICR), which is the basis of all Ca^{2+} signals discussed here.

We focus on two properties of Ca^{2+} signals that have been studied recently:

- *Subcellular organization*. The multiple intracellular spatial scales and a related hierarchy of collective behavior (Berridge et al. 2003) shape the signals of Ca^{2+} (Fig. 4.1). This fact becomes apparent since release events at the different scales can be associated with different functional roles in cellular communication. The smallest events in the Ca^{2+} signal hierarchy are short-lived openings of single channels called blips. Experimental observation of larger, yet still localized release events called puffs (Parker and Yao 1996) indicates that functioning IP_3R channels are grouped into clusters on the ER membrane containing at most tens of channels. Their opening is the result of local diffusion of Ca^{2+} and CICR between adjacent channels. Ca^{2+} signals therefore often exhibit spatial gradients, which have been shown to be important in the signaling content of Ca^{2+} signals for gene expression (Di Capite et al. 2009). The significance of the nanodomain distribution for Ca^{2+} function has also been shown recently in dendritic spines, where it was found that RyR channels are present in the postsynaptic dendritic spine (Johenning et al. 2015). Here, the channels play a role in synaptic plasticity but can do so only if a local concentration is raised above the Ca^{2+} elevation in the spine. Finally, the largest scale of Ca^{2+} signals is produced by whole-cell oscillations and waves, which are observed in many cell types. These signals are believed to comprise release from many clusters and possibly from further isolated channels situated between the clusters (Smith et al. 2009).
- *Stochasticity*. It was found that puffs, lasting from 50 to a few hundreds milliseconds, are strongly stochastic events (Marchant and Parker 2001). The most obvious source of noise for puffs is the small number of channels within a cluster (around 3–30). Several mathematical models have been put forward that reproduce the stochastic and dynamic features of puffs based on the single channel gating noise (e.g. Shuai and Jung 2003; DeRemigio et al. 2008; Rüdiger et al. 2010a). Furthermore, experiments have shown that global oscillations also have a strong stochastic component. Attributing this noise again to intrinsic stochastic behavior, fluctuations in the interwave interval have been associated with single channel noise in a number of computational models (Falcke 2003; Skupin et al. 2010; Rückl et al. 2015).

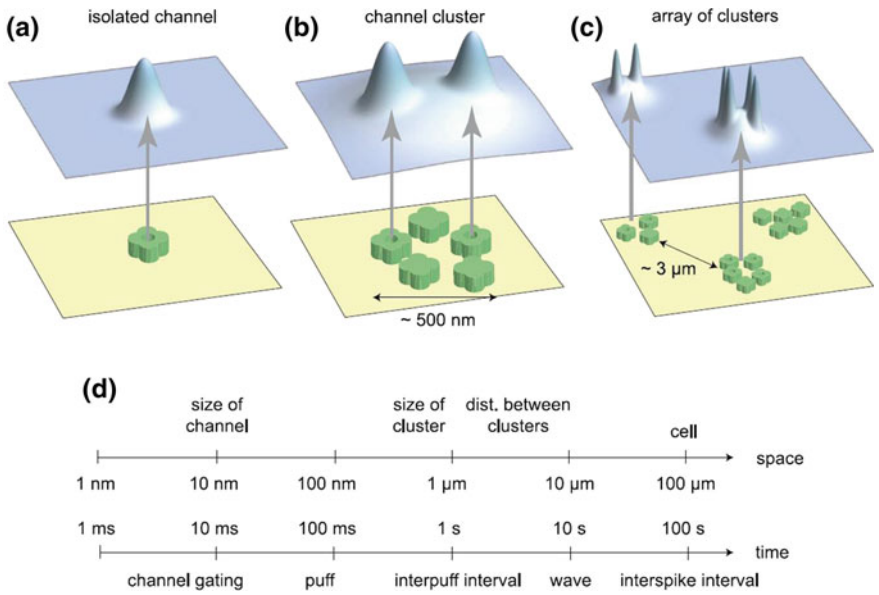

Fig. 4.1 The multiple spatial and time scales of Ca^{2+} signals (Rüdiger 2014a). **a** Ca^{2+} blips released from a single channel, **b** Ca^{2+} puffs released from several channels in a cluster, **c** Ca^{2+} signals released from an array of clusters. **d** An overview of the relevant scales in space and time

In early modeling studies, time-dependent Ca^{2+} elevations were described using deterministic ordinary differential equations (ODEs). These were based on a small number of feedback processes, the combination of which can indeed guarantee the existence of a limit cycle behavior. However, the two properties that we have mentioned, spatial localization and noise, require more complex spatial, nonlinear and stochastic equations, of the kind not usually studied in standard systems biology. Studies have resulted in evidence that the Ca^{2+} oscillator belongs to the class of stochastic excitable systems and not to the limit cycle class. In the following section we review a number of approaches to the problem, including partial differential equations (PDEs), Markovian modeling and numerical methods. In each case, we discuss the links to recent experimental results.

4.2 Stochastic Simulation of IP3R Gating Dynamics

4.2.1 Master Equations of the Stochastic Process

First, we discuss a toy model of a channel with the following open and close processes only

$$\mathrm{C} \underset{\beta}{\overset{\alpha}{\rightleftharpoons}} \mathrm{O} \tag{4.1}$$

with the open rate α and the closing rate β. Given a large ensemble of channels, the differential equations for the state fractions x_i of channels ($i = o$ or c) can be given. For example, the open fraction x_o is written as,

$$\frac{dx_o}{dt} = \alpha(1 - x_o) - \beta x_o \tag{4.2}$$

Equation 4.2 is suitable for a large numbers of channels with continuous state fractions. However, when the channel number is small, the state fractions become discrete. The fluctuations of the channel number in the states i around its mean values become large, and the standard deviation around the mean value is of the order $1/\sqrt{N}$ with N the total channel number. As a result, the above differential equation based on the law of mass action needs to be replaced by the corresponding master equations, where the reactions are treated as Markovian birth-death processes. Taking M to be the number of open channels, one has the following master equation:

$$\begin{aligned}\frac{\mathrm{d}P(M,t)}{\mathrm{d}t} &= \alpha((N - M + 1)P(M - 1, t) - (N - M)P(M, t)) \\ &\quad +\beta((M + 1)P(M + 1, t) - MP(M, t)),\end{aligned} \tag{4.3}$$

where $P(M, t)$ is the probability of having M open channels at time t.

The master equations can be solved in an analytical way only for simple cases. This is not practical in the case of more complex master equations involving many channels or many different receptor states. Thus, numerical methods are usually required to solve the master equations for complex gating states. For instance, a widely discussed IP_3R channel model based on the microscopic kinetics of IP_3 and Ca^{2+} gating was proposed by DeYoung and Keizer (1992). The model assumes that three equivalent and independent subunits are involved in conduction of an IP_3R. Each subunit has one binding site for IP_3 (gate m) and two binding sites for Ca^{2+}: one Ca^{2+}-binding site for activation (gate n), the other for inhibition (gate h). The subunit conducts only when the IP_3 site and activation Ca^{2+} site are bound. Thus, as shown in Fig. 4.2a, each subunit may exist in eight states with transitions governed by the first- or second-order rate constants. For such a subunit-based model with three types of binding sites, we need to determine the evolution of a probability density $P(M_m, M_n, M_h, t)$ in a three-dimensional occupation number space. For the channel-based model, the probability density in an even larger space must be tracked. In this case, solutions can be obtained by Monte Carlo methods, where exemplary trajectories are calculated using random numbers in a way appropriate to the transition rates. Single trajectories can then be collected to obtain statistical features of the system.

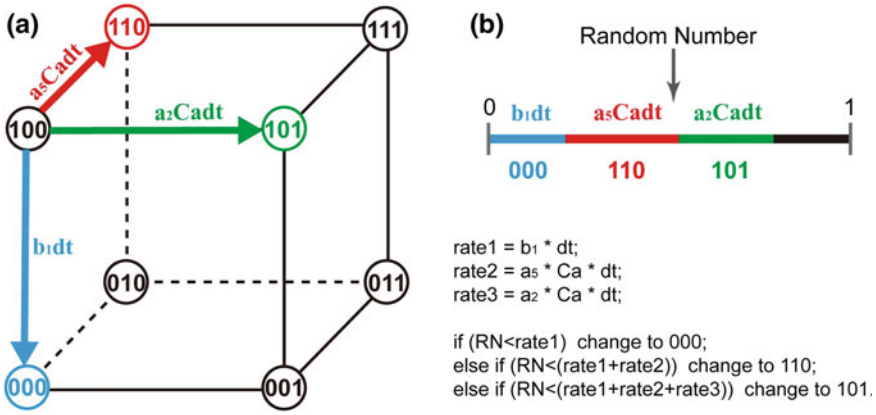

Fig. 4.2 **a** The eight IP_3R subunit states proposed by DeYoung and Keizer (1992). **b** An example to show how the two-state Markovian method simulates the stochastic gating dynamics from the current (100)-state to the three other possible states of (000), (110), or (101) (see also Chap. 3)

4.2.2 Gillespie Simulation

A mathematically precise basis for stochastic simulation algorithms was derived by Gillespie (1976, 1977). The approach relies on the notion of a propensity a_i for each microscopic transition or reaction R_i. Then

$$a_i \mathrm{d}t = h_i c_i \mathrm{d}t \tag{4.4}$$

is the probability that reaction R_i occurs during the next infinitesimal time step $\mathrm{d}t$. Here c_i denotes the reaction constant of R_i (the probability density that a combination of molecules reacts) and h_i is the number of particle combinations of that particular reaction. For instance, in the case of a mono-molecular reaction, $A \rightarrow B$, h equals X_A, where X_A is the number of A-molecules in a certain well-mixed volume V, and c equals the macroscopic rate k of the transition. Similarly, for $A + B \rightarrow 2A$, $h = X_\mathrm{A} X_\mathrm{B}$ and the macroscopic $k = cV$. If a reaction is called, the corresponding numbers of participating molecule species, X_j, $j = 1, \ldots, K$, are updated according to the stoichiometric factors, which are conveniently placed into a matrix, ν_{ij}, defined as

$$\begin{aligned} \nu_{ij} \equiv & \text{ change in the number of } X_j \text{ molecules produced} \\ & \text{by one } R_i \text{ reaction.} \end{aligned} \tag{4.5}$$

The stochastic algorithm determines the time of the next reaction and which reaction it will be, given the state $\boldsymbol{X} = (X_\mathrm{A}, X_\mathrm{B}, \ldots)$ at the starting time t. Let

$P_0(\tau)$ be the probability that no reaction will occur in $(t, t+\tau)$ and $a_i = a_i(\boldsymbol{X})$ the propensity at time t. Since $1 - \sum_i a_i \mathrm{d}\tau$ is the probability that no reaction will occur in $\mathrm{d}\tau$, where the sum's index runs over all reactions, we find that

$$P_0(\tau + \mathrm{d}\tau) = P_0(\tau)\left(1 - \sum_i a_i \mathrm{d}\tau\right) \tag{4.6}$$

is the probability that no reaction has occurred in $(t, t+\tau+\mathrm{d}\tau)$. The last equation implies that $P_0(\tau) = \exp(-\sum_i a_i \tau)$. On the other hand, the probability that the next reaction is R_i and it occurs in $(t+\tau, t+\tau+\mathrm{d}t)$ is $P(\tau, i)\mathrm{d}t = P_0(\tau)a_i \mathrm{d}t$, *i.e.*,

$$P(\tau, i) = a_i \exp(-a_0 \tau), \tag{4.7}$$

where $a_0 = \sum_i a_i$ is the sum of all propensities. The probability density $P(\tau, i)$ can be implemented by drawing two random numbers r_1 and r_2 from a uniform distribution in the interval [0, 1], and choosing τ and i such that

$$a_0 \cdot \tau = \ln(1/r_1), \qquad \sum_{j=1}^{i} a_j \le a_0 \cdot r_2 < \sum_{j=1}^{i+1} a_j. \tag{4.8}$$

This algorithm determines which reaction R_i is executed in the next step and when it will occur (time τ). This method is the so-called Direct Method (Gillespie 1976). Variants, which differ in the application of random numbers, are the First (Gillespie 1976) and Next Reaction Methods (Gibson and Bruck 2000).

The numerical effort can be substantially reduced if there is a strong disparity in the amplitude of noise in various parts of the reaction system. If some of the reactants are strongly fluctuating in their number, while others evolve more regularly, the system can be split into a stochastic part simulated with one of the methods described above, and a deterministic part solved by numerical schemes for differential equations. Both parts then need to be linked in an appropriate way. Previous research followed a strategy where fast reactions are represented by the deterministic rate equation, while slow reactions are treated with the exact stochastic algorithm. An example is the stochastic simulation of the Li-Rinzel Ca^{2+} model (Li and Rinzel 1994), as discussed below.

In a similar manner, the evolution of calcium concentration can be treated deterministically, while the gating transitions of ion channels need to be simulated stochastically. However, when combining a deterministic evolution with a stochastic solver, one may encounter the following problem. Gillespie's method rests on the assumption that during successive stochastic events, the propensities a_i do not change (Gillespie 1976, 1977; Gibson and Bruck 2000). However, when linking the stochastic reaction dynamics to the deterministic dynamics, we expect the propensity of a_i to change over time due to its dependence on deterministic variables. This effect, as seen below, will be particularly strong for the opening and closing of channels, since after such events the local calcium concentration changes dramatically by three or four orders of magnitude.

One way to resolve this problem was introduced by Alfonsi et al. (2005) and applied to the Ca^{2+} system (Rüdiger et al. 2007). Within this setting, the time τ to the next stochastic event is determined by solving

$$\int_t^{t+\tau} a_0(s, c)\, \mathrm{d}s = \chi, \tag{4.9}$$

with $\chi = \ln(1/r_1)$, where the sum of propensities a_0 may depend explicitly on both time s and deterministic variables, here denoted by c. The above equation simplifies to the equation determining τ in (4.8) for a constant a_0. To determine the time τ of the next reaction, condition (4.9) is conveniently rewritten in differential form by introducing a variable $g(\tau)$ and solving

$$\dot{g}(s) = a_0(s, c) \tag{4.10}$$

with initial condition $g(t) = 0$, along with the differential equations for deterministic variables. A reaction occurs whenever $g(s)$ reaches the random number χ. As before, the specific event R_i is determined based on a second random number r_2 satisfying the second condition in Eq. (4.8) with propensities evaluated at the event time $t + \tau$.

4.2.3 Two-State Markovian Method

As an alternative, solutions can be obtained by a simple two-state Markovian method. By expanding the transition probabilities at the linear order for the small time step δt, one can obtain the transition probability P of hopping from i-state to j-state within δt

$$P(i|j, \delta t) = \delta t \times \gamma_{ji} \tag{4.11}$$

with the rate γ_{ji} from i-state to j-state, and the probability to remain in the same state

$$P(i|i, \delta t) = 1 - \delta t \times \sum_j \gamma_{ji} \tag{4.12}$$

This scheme can be expressed directly in terms of a computer algorithm. In detail, the channel state is updated for every small time step δt. For the toy model (4.1), if the channel is closed at time t, the probability that it becomes open at time $t + \delta t$ is $\alpha \cdot \delta t$. If it is open at time t, then the probability that it becomes closed at time $t + \delta t$ is $\beta \cdot \delta t$.

Such a two-state Markovian method can by applied easily to the complex DeYoung-Keizer IP_3R model (DeYoung and Keizer 1992). Generally, to determine the state of a channel, random numbers from a uniform distribution on the unit interval [0, 1] are drawn. Each transition represents a subinterval on the unit interval proportional to the value of its transition probability where the sum of all subintervals

represents possible transitions. The transition that corresponds to the subinterval into which the random number falls is actually performed in simulation. An example is how the two-state Markovian method simulates the stochastic gating dynamics from the current (100)-state to the three other possible states of (000), (110), or (101) is explained in Fig. 4.2b.

4.2.4 Gate-Based Langevin Approach

For a large number of channels N, the master equation can be approximated by a Fokker-Planck equation, which is a linear partial differential equation. For every Fokker-Planck equation there is a statistically equivalent set of Langevin equations, i.e., a set of stochastic differential equations (Fox and Lu 1994).

As an example, we discuss the Langevin approach of the Li-Rinzel Ca^{2+} model (Li and Rinzel 1994) which is a simplified DeYoung-Keizer model (DeYoung and Keizer 1992) with two variables only (Chap. 3):

$$\frac{\mathrm{d}C}{\mathrm{d}t} = J_r(C,h,I) + J_l(C) - J_p(C), \tag{4.13}$$

$$\frac{\mathrm{d}h}{\mathrm{d}t} = \frac{h-h_\infty}{\tau_h} = \alpha_h(1-h) - \beta_h h, \tag{4.14}$$

with C the intracellular Ca^{2+} concentration, I the IP_3 concentration, and h the fraction of deinactivated IP_3Rs. The first term J_r in Eq. (4.13) denotes the channel flux density from the ER into the intracellular space, the second term J_l is the leak flux density and the third term J_p is the pump flux density from the intracellular space into the ER (Fig. 4.3). Equation (4.14) for h defines the fractions of the subunits in deinhibited states.

The expressions for the fluxes are given by

$$J_r = \Omega_C\, m_\infty^3\, h^3\, (C_T - (1+\rho_A)C)\,, \tag{4.15}$$

$$J_p = O_P\, \mathcal{H}_2\,(C, K_P)\,, \tag{4.16}$$

$$J_l = \Omega_L\,(C_T - (1+\rho_A)C)\,, \tag{4.17}$$

with the parameters given as

$$\begin{aligned} m_\infty &= \mathcal{H}_1\,(I,d_1)\cdot\mathcal{H}_1\,(C,d_5)\,,\\ \alpha_h &= \frac{h_\infty}{\tau_h} = O_2 Q_2,\\ \beta_h &= \frac{1-h_\infty}{\tau_h} = O_2 C,\\ Q_2 &= d_2\frac{I+d_1}{I+d_3}. \end{aligned} \tag{4.18}$$

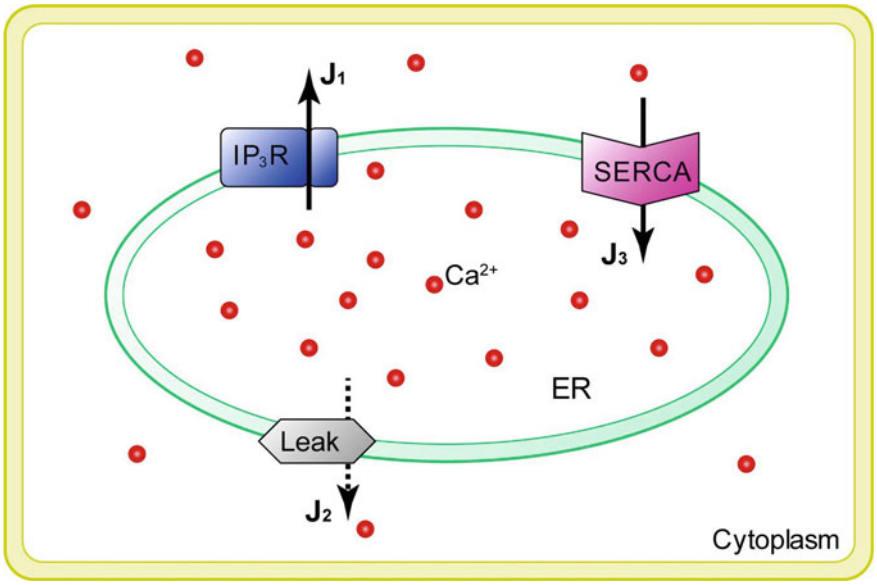

Fig. 4.3 The scheme of the Ca^{2+} oscillation model. Intracellular Ca^{2+} is controlled by channel flux as well as a leak flux from the ER into the intracellular space and the pump flux from the intracellular space into the ER

The parameters of the model are $\rho_A = 0.185$, $\Omega_C = 1.11\ s^{-1}$, $\Omega_L = 0.02035\ s^{-1}$, $O_P = 0.9\,\mu M\,s^{-1}$, $K_P = 0.1\,\mu M$, $d_1 = 0.13\,\mu M$, $d_2 = 1.049\,\mu M$, $d_3 = 0.9434\,\mu M$, $d_5 = 0.08234\,\mu M$, and $O_2 = 0.2\,\mu M^{-1}\,s^{-1}$ (Li and Rinzel 1994). Conservation of Ca^{2+} implies the constraint of Ca^{2+} concentration in ER $C_E = C_T - \rho C$ with $C_T = 2\rho\ \mu M$. The concentration I is a control parameter.

Equations (4.13) and (4.14) describe the deterministic behavior averaged for a large number of channels. The small number of IP_3Rs in a single cluster suggests that a stochastic formulation of these equations is necessary if calcium release from a single cluster should be considered.

Following the deterministic Li-Rinzel model, one can consider the stochastic opening and closing process only for the gate h. Each gate h is an inactive binding site for Ca^{2+} which is occupied (closing) or non-occupied (opening). We describe the binding and unbinding of these three sites using an independent two-state Markov processes with opening and closing rates α_h and β_h, respectively.

One can simply assume that the stochastic dynamics of the IP_3R channels can be reflected by the fluctuation of the open fraction of channel subunit h. As a result, the Langevin equation for the fraction of the h-open subunit is expressed as (Shuai and Jung 2002)

$$\frac{dh}{dt} = \alpha_h(1-h) - \beta_h h + G_h(t) \tag{4.19}$$

where $G_h(t)$ are zero mean, uncorrelated, Gaussian white-noise terms with

$$\langle G_h(t)G_h(t')\rangle = \frac{\alpha_h(1-h)+\beta_h h}{N}\delta(t-t'), \tag{4.20}$$

Such a gate-based Langevin approach indicates that the stochastic dynamics of the IP_3R open fraction can be treated as a deterministic dynamics disturbed by a Gaussian white noise.

In the simulation, the Gaussian noise sources are generated at each integration step by the Box-Muller algorithm. For example, we can simply use the Euler integration to solve the deterministic terms. Let the time step be δt, and γ_1 and γ_2 be two uniformly distributed random numbers in (0, 1]. The Box-Muller algorithm requires that one should add the following noise term into the Euler integration (Fox 1997)

$$g_h = \sqrt{-2\frac{\alpha_h(1-h)+\beta_h h}{N}\log(\gamma_1)}\sin(2\pi\gamma_2) \tag{4.21}$$

As a result, the Euler integration of the Langevin equation for the Li-Rinzel model is given as

$$h(t+\delta t) = h(t) + \delta t(\alpha_h(1-h) - \beta_h h) + g_h(t)\sqrt{\delta t} \tag{4.22}$$

Since h has to be bound between 0 and 1, it is necessary to verify this condition after each iteration step. The approximate nature of Eq. 4.19 does not automatically maintain h in the required interval. One can simply put the value of h as 0 or 1 when it it is out of [0, 1]. Simulation shows that the results are insensitive to the choice of strategy used to keep h in [0, 1].

Instead of applying three identical h-gates with h^3 in Eq. (4.15), one can also consider three independent h-gates with $h_1h_2h_3$ in Eq. (4.15) which are disturbed individually by different Gaussian white noises (Shuai and Jung 2002; Huang et al. 2011).

4.2.5 Channel-Based Langevin Approach

Consisting of three subunits for IP_3R of the Li-Rinzel model, each channel has four possible h-uninhibited states, as shown in Fig. 4.4. Define state fraction x_i as the rate of the channel number in i h-uninibited state among the total channel number with $i = 0, 1, 2, 3$. The stochastic channel kinetics can be modeled as a four-state Markov chain dynamics. Applying a vector $\mathrm{X} = \{x_i\}$ to represent the four state fractions, the evolution of channel state fractions can be traced by the following channel-based Langevin equation (Fox 1997; Huang et al. 2011)

$$\frac{d\mathbf{X}}{dt} = A\mathbf{X} + \frac{S}{\sqrt{N}}\xi, \tag{4.23}$$

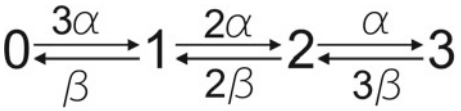

Fig. 4.4 Transition diagram of IP_3R channel state. The number indicates how many subunits in the channel are in the h-uninhibited state

where A is the transition matrix representing the transition dynamics between different channel states. Based on the Markovian chain shown in Fig. 4.4, one has

$$A = \begin{pmatrix} -3\alpha & \beta & 0 & 0 \\ 3\alpha & -2\alpha-\beta & 2\beta & 0 \\ 0 & 2\alpha & -\alpha-2\beta & 3\beta \\ 0 & 0 & \alpha & -3\beta \end{pmatrix} \tag{4.24}$$

In Eq. (4.23), the matrix S is the square root matrix of diffusion matrix $D = SS^T$ which is given by

$$D = \begin{pmatrix} 3\alpha x_0 + \beta x_1 & -3\alpha x_0 - \beta x_1 & 0 & 0 \\ -3\alpha x_0 - \beta x_1 & 3\alpha x_0 + (\beta+2\alpha)x_1 + 2\beta x_2 & -2\alpha x_1 - 2\beta x_2 & 0 \\ 0 & -2\alpha x_1 - 2\beta x_2 & 2\alpha x_1 + (\alpha+2\beta)x_2 + 3\beta x_3 & -\alpha x_2 - 3\beta x_3 \\ 0 & 0 & -\alpha x_2 - 3\beta x_3 & \alpha x_2 + 3\beta x_3 \end{pmatrix} \tag{4.25}$$

The vector ξ in Eq. (4.23) is a noise term with four elements. Each noise element is a Gaussian white noise with zero means and unit variances.

As a result, instead of Eq. (4.15) for channel flux, we have the following expressions for channel flux

$$J_r = \Omega_C \, m_\infty^3 x_3 \, (C_T - (1+\rho_A)C) \tag{4.26}$$

in which x_3 is the h-open fraction of channels. Due to the Gaussian noise terms added, channel state fractions are no longer guaranteed to lie on the bounded domain, but have a probability to violate the meaningful interval [0, 1]. One can allow for the means of simplicity that fractions evolve unboundedly, and for values outside [0, 1] the positive semidefiniteness of the diffusion matrix may not be given thus hindering the computations of the matrix square roots. One can also keep the boundary limitation of [0, 1] by simply putting $x_i = 0$ or 1 once they are out of the bound and calculate $x_0 = 1 - \sum_{i>0} x_i$ to ensure $\sum x_i = 1$. Some better but complex constraining methods have also been proposed (Huang et al. 2013).

Orio et al. proposed a simple structure of the square root matrix to solve the stochastic differential equations of the Hodgkin-Huxley neuronal model (Orio and Soudry 2012), which can also be applied here to the Li-Rinzel Ca^{2+} model. In this approach, the Cholesky decomposition was extended to solve the stochastic terms of complex kinetic schemes of the four-state channel. In detail, the random term for i is equal to the square root of the sum of the forward ($i \to j$) and backward

$(i \leftarrow j)$ transition probabilities for the transition pair $i \leftrightarrows j$, scaled by the inverse of the channel number. As a result, one has

$$\frac{d\mathbf{X}}{dt} = A\mathbf{X} + S^O\xi, \tag{4.27}$$

Here, the square root matrix S^O in Eq. (4.27) is directly given by

$$S^O = \frac{KF}{\sqrt{N}} \tag{4.28}$$

where K is a 4×3 matrix given by

$$K = \begin{pmatrix} 1 & 0 & 0 \\ -1 & 1 & 0 \\ 0 & -1 & 1 \\ 0 & 0 & -1 \end{pmatrix} \tag{4.29}$$

and F is a 3×3 diagonal matrix with the diagonal elements given by

$$\mathrm{diag}(F) = \begin{pmatrix} 3\alpha x_0 + \beta x_1 \\ 2\alpha x_1 + 2\beta x_2 \\ \alpha x_2 + 3\beta x_3 \end{pmatrix}$$

Such a simple expression for the square root matrix naturally fulfills the requirement of $SS^T = D$. Note that $\mathbf{X}$ is a vector with four elements, but ξ here it is a noise vector with only three elements and S^O is a 3×4 matrix. With the method proposed by Orio and Soudry (2012), the expensive matrix square root calculation is avoided, largely reducing the total computational cost during the numerical simulation.

4.3 Stochastic Ca^{2+} Puff Dynamics

4.3.1 Limitation of Modeling with Homogeneous Ca^{2+} Concentration Within IP_3R Clusters

One can simply use the Markov version of the Li-Rinzel model (Li and Rinzel 1994) to study the statistical properties of Ca^{2+} puffs released from a cluster of IP_3Rs with stochastic gating dynamics. In this simple stochastic Li-Rinzel model, spatial aspects of the formation and collapse of localized Ca^{2+} elevations are ignored. The Ca^{2+} diffusion between the cluster and the environment is ignored so that an isolated cluster can be discussed. On the other hand, the channels are assumed to be close enough and the instantaneous Ca^{2+} diffusion within a cluster to be so fast that the

calcium concentration within a cluster is assumed to be always homogeneous. The small size of the IP_3R clusters introduces strong stochasticity for puffs, resulting in a distribution of puff amplitude, lifetime and inter-puff interval (Shuai and Jung 2002).

However, experimental and theoretical work (Roberts 1994; Rüdiger et al. 2007) suggests that even at steady state the Ca^{2+} diffusion at a Ca^{2+} release site may lead to inhomogeneous profiles even in a very small region. Simply assuming that the ER membrane acts as a flat boundary to limit the Ca^{2+} diffusion in a half three-dimensional space and Ca^{2+} ions diffuse from a point release source of IP_3Rs, a solution of the linearized reaction-diffusion equation indicates that a sharp distribution around the release point can be established (Smith 1996; Neher 1998),

$$c(r) = \frac{I_{IP3R}}{4\pi r F D_{Ca}} \exp(-r/\lambda) + c_0, \tag{4.30}$$

where I_{IP3R} is the current of IP_3R, D_{Ca} is the diffusion coefficient for free Ca^{2+}, and c_0 is the Ca^{2+} concentration at resting state. The parameter λ is an important factor which accounts for the Ca^{2+} diffusion and binding to buffers. The term $\exp(-r/\lambda)/r$ indicates that the decay of Ca^{2+} concentration with distance is even sharper than the exponential function.

As shown in Fig. 4.5, a numerical simulation with the finite element method shows a sharp decay of the stationary Ca^{2+} concentration against distance from the channel center. The Ca^{2+} concentration at the channel pore is about 110 µM. It decreases to about 20 µM at a distance of 15 nm which is about the size of the IP_3R channel, and decreases to about 0.7 µM at a distance of 200 nm, which is about the size of the IP_3R cluster. These data indicate that the homogeneous Ca^{2+} concentration for clustered IP_3Rs is not a suitable assumption, for a puff simulation with a cluster size of a few hundred nanometers.

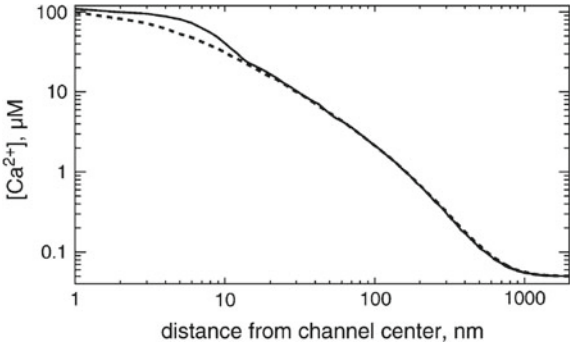

Fig. 4.5 The stationary Ca^{2+} concentration against distance for an open channel directly along the ER membrane (solid) and perpendicular to the membrane (dashed) as calculated with finite element discretization (Rüdiger et al. 2010b)

4.3.2 *Two-Scale Modeling of Ca^{2+} Concentration Within IP_3R Clusters*

Considering the sharp decay around the open channel, a puff model with two-scale Ca^{2+} concentration was proposed (Rüdiger et al. 2010a). In fact, if a channel is open, the local Ca^{2+} concentrations reach values above 100 μM, while closed channels in a cluster are subjected to much lower concentrations. For simplicity, one may introduce a domain Ca^{2+} concentration for all the closed channels in a cluster. As shown in Fig. 4.6b, it can be seen that the domain Ca^{2+}, c_d, can be well described by a linear relationship with the number of open channels, n as

$$c_{\mathrm{d}}(n) = c_0 + c_1 n, \tag{4.31}$$

where c_0 is the rest level concentration and c_1 is a coupling constant (Rüdiger et al. 2010a).

The dynamics for N channels in a cluster can then be simulated by using discrete Markovian gating transitions and using equations for the Ca^{2+} concentration such as Eq. (4.31). Various schemes have been studied and have been shown to produce Ca^{2+} dynamics resembling experimentally observed Ca^{2+} puffs (DeRemigio et al. 2008; Rüdiger et al. 2010a; Cao et al. 2013; Rüdiger 2014b).

When a channel switches from the open state to the closed state, the domain Ca^{2+} concentration will be influenced by its diffusion and binding and unbinding with various buffers before it reaches the equilibrium value c_{d}. To incorporate the collapsing dynamics, one can consider the following differential equation for c_{d} around the closed channels (Rüdiger et al. 2014)

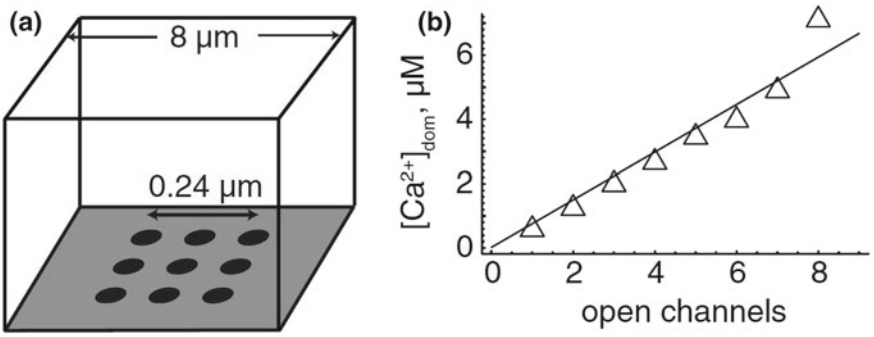

Fig. 4.6 FEM simulation of Ca^{2+} release from nine channels in a cluster (Rüdiger et al. 2010a). **a** The box of dimension $8 \times 8 \times 5\mu m^3$ represents the cytosolic space. Channels are located on the ER membrane. **b** The domain calcium concentrations are obtained by averaging the closed channels for a given total number of open ones

$$\frac{dc_d}{dt} = \gamma(c_0 + c_1 n - c_d). \tag{4.32}$$

Here γ is the decay rate for the domain Ca^{2+} collapse, which in general depends on many factors such as cluster size and buffer content. As an example, the temporal evolution of the open channel number and the corresponding cluster domain Ca^{2+} is given in Fig. 4.7. The stochastic channel opening and closing in the cluster causes the occurrence of puffs and blips.

To further address the possible equivalence within a differential equation approach, one needs to replace n in Eq. (4.31) with the product of the total number of channels, N, and the fraction of channels in the open state a. Substituting the discrete number of channels for its continuous counterpart, Na, entails that c_d can be larger than c_0 even if less than one channel is open. This misrepresentation is a source of inadequate continuous modeling and in Rüdiger (2014b) a function that possesses a step at the crucial transition from zero to one open channel was introduced:

$$c_d(a) = c_0 + c_1 Na \frac{1}{2}[1 + \tanh((Na - 1)/\epsilon))]. \tag{4.33}$$

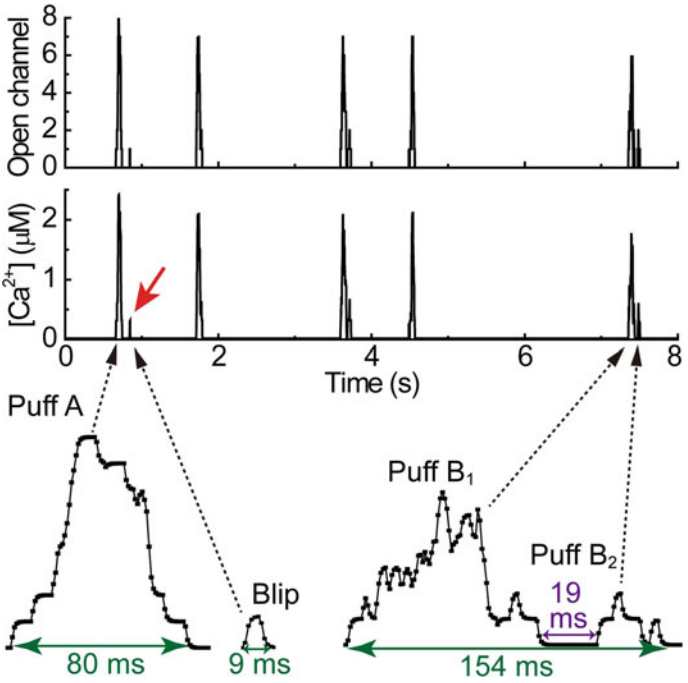

Fig. 4.7 The temporal evolution of open channel number (top) and the corresponding cluster domain Ca^{2+} (middle). The arrow marks a blip. Two puffs (Puff A and Puff B) and a blip are depicted in the enlarged drawing (bottom) (Qi et al. 2015)

Here, the parameter ϵ characterizes the "discreteness" of the 0-1 step and was chosen as 0.1 in Rüdiger (2014b).

4.3.3 *Puff Dynamics in a Langevin Model*

In Rüdiger et al. (2010a) a Markov chain of four states was used, which basically represent the four states obtained from activation and inhibition, see Fig. 4.8. The simulations based on this scheme and other schemes suggested a dynamics similar to the excitable behavior well known from models for neuronal action potentials including the Hodgkin-Huxley equations (Hodgkin and Huxley 1952).

Rate equations with Langevin noise for each gating state can be derived from the reaction scheme in the standard way (Shuai and Jung 2003). For example, the fraction of channels in the state a is given by

$$\frac{\mathrm{d}a}{\mathrm{d}t} = k_{\mathrm{a}}^{+} cz - k_{\mathrm{a}}^{-} a + k_{\mathrm{i}}^{-} g - k_{\mathrm{i}}^{+} c_{\mathrm{s}} a + G_{\mathrm{za}} + G_{\mathrm{ag}}. \tag{4.34}$$

The $G_{..}$ terms are Langevin noises representing stochasticity of channel opening/closing. Following the approach of Fox and Lu (1994) one obtains, for instance, for $G_{\mathrm{za}}(t)$ a zero mean, Gaussian white noise term with $\langle G_{\mathrm{za}}(t) G_{\mathrm{za}}(t') \rangle = (k_{\mathrm{a}}^{+} c_{\mathrm{d}} z + k_{\mathrm{a}}^{-a}) \delta(t - t')/N$. In Rüdiger (2014b) these equations were simulated together with ODEs for the cluster domain Ca^{2+} concentration. It was found that an excitable trajectory, similar to those in other systems such as action potentials in the FitzHugh-Naguma system, underlies the puff dynamics, see Fig. 4.8b.

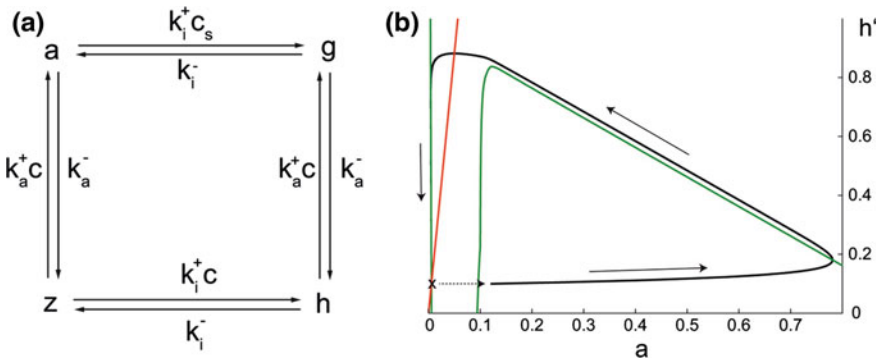

Fig. 4.8 **a** Four-state model based on single channel activation and inhibition. The rest state is denoted by z. Activation of the channel by Ca^{2+} binding corresponds to its opening (state a). Further Ca^{2+} binding results in the closing of the channel (states g and h). **b** Excitable trajectory (solid black line) in a two-dimensional ODE based on the model shown in (**a**) and Eq. (4.33). Here the green and red lines show the nullclines of the activator and inhibitor variables, respectively Adapted from Rüdiger (2014b)

4.3.4 Ca^{2+} Dynamics with Clustered Channels in a 3D Model

Ca^{2+} release from a group of IP_3R channels has also been studied in three-dimensional models of the cytosolic space. The main problem encountered here is the strongly localized distribution of Ca^{2+} within the cell, which requires a very high spatial resolution in numerical modeling. Related to the clustering of IP_3R channels, there are two basic domain sizes to be considered. It was first recognized that the clustering of channels and release of Ca^{2+} produces a local elevation of Ca^{2+} to values between 1 and 10 μM. The spatial extent of these domains roughly follows that of the cluster (less than or close to 1 μM) and hence the domains are called microdomains. It was therefore suspected that the microdomain provides a homogenous local reaction space, so that all Ca^{2+} channels within the domain "feel" equal Ca^{2+} concentrations. Later, however, using more advanced methods of numerical spatial discretization, it appeared that Ca^{2+} is distributed very unevenly within a microdomain. This follows from the evidence that channels within a cluster are distanced at a few tens or hundreds of nm, so that after the opening of channels, gradients of $[Ca^{2+}]$ (roughly $1/r$, where r is the radial distance from the channel pore) result. Thus, around an open channel, values of concentration of up to hundreds of μM result, while the concentrations at adjacent channels due to the open channel are much lower. Hence for a realistic modeling of local Ca^{2+} signals the assumption of a common reaction space for all channels is not valid (Rüdiger et al. 2010a).

An accurate description of intracellular Ca^{2+} dynamics takes into account Ca^{2+} diffusion and binding to buffers as well as transport to and from the intracellular storage compartments, mainly in the ER. Diffusion of Ca^{2+} and binding of Ca^{2+} to buffer proteins or endogenous buffers is modeled by reaction-diffusion equations, while transport through the ER membrane is given by influx conditions on the ER surface. In the following we consider the sample case of one buffer only, where c and b respectively denote the free cytosolic and bound buffer Ca^{2+} concentrations. Assuming simple reaction kinetics this leads to the following system of PDEs:

$$\frac{\partial c}{\partial t} = D_c \nabla^2 c + b\, k^- - c\, k^+ (B - b) \tag{4.35}$$

$$\frac{\partial b}{\partial t} = D_b \nabla^2 b - b\, k^- + c\, k^+ (B - b). \tag{4.36}$$

D_c, D_b and B denote the diffusion coefficients of free Ca^{2+}, bound buffer and the total buffer concentration, respectively.

The equations are solved within a domain denoted Ω as shown below. Influx through the channels is given by boundary conditions on the domain boundary $\partial\Omega_M$ that represents the ER membrane:

$$D_c \vec{n}\, \vec{\nabla} c = \begin{cases} J, & \text{at } \partial\Omega_M \\ 0, & \text{at } \partial\Omega \setminus \partial\Omega_M \end{cases} \tag{4.37}$$

$$D_b \vec{n}\, \vec{\nabla} b = 0, \text{ at } \partial\Omega. \tag{4.38}$$

Here, $\vec{n}$ denotes the outer normal vector of the boundary of the domain denoted by $\partial\Omega$. J describes the flux through the ER membrane and comprises three contributions:

$$J = P_c S(\vec{r}, t)(E - c) - P_p \frac{c^2}{K_d^2 + c^2} + P_l(E - c), \tag{4.39}$$

where $\vec{r} = (x, y, z)$ denotes the spatial position on the membrane and E is the $[Ca^{2+}]$ in the ER lumen. Since the ER was estimated to not be depleted during puffs (Ullah et al. 2012), one often assumes E to be constant.

The first term on the rhs of Eq. (4.39) models current through the IP_3R channels from the ER to the cytosol. This term is controlled by the channel state through the factor $S(\vec{r}, t)$, which is non-zero in small areas representing the open channels. The source areas should be chosen to be small to realistically model pore regions and the large Ca^{2+} gradients around open channels.

The second term in Eq. (4.39) models SERCA pumps. Standard models such as the one in Eq. (4.39) are of the Hill equation type with Hill coefficient 2 (Lytton et al. 1992). K_d is the dissociation constant of the pumps. The maximal pump current, V_p, was estimated to be 10–16 $\mu M\, s^{-1}$ (Falcke 2004). This number is based on a volume source and needs to be cast into a flux through a boundary by multiplying the volume current by the domain extension d_z. This results in units of moles per surface area and time, as is required for the boundary flux.

The last term in Eq. (4.39) models a small leakage of Ca^{2+} from the luminal to the cytosolic domain. Besides its physiological relevance, it also serves to balance the system in the rest state, i.e., it compensates the SERCA pumps when there are no open channels. To achieve a resting $[Ca^{2+}]$ of a few tens of nM (c_0) in the cytosolic domain and a few hundreds of μM in the ER (E), equating the two last terms of Eq. (4.39) provides a dependence of P_l on P_p:

$$P_l = \frac{P_p c_0^2}{(E - c_0)\left(K_d^2 + c_0^2\right)}. \tag{4.40}$$

Due to the multiple spatial scales, special care has to be given to spatial discretization in the numerical schemes. In one line of research, three-dimensional simulation software (Rüdiger et al. 2007, 2010b; Rückl et al. 2015) was established using the finite element method. The PDE-solver is based on locally grid-adapted finite elements in space that resolve the extreme spatial gradients of Ca^{2+} concentrations around an open channel. Typically, a spatial grid of less than 1 nm is needed in the close neighborhood of a channel, while the grid distance relaxes to around 500 nm further from the channels.

The stochastic gating transitions are described by schemes defining the states, the transitions and transition rates. As described above, the standard method to numerically time-advance such states' variables is the Gillespie method. The Gillespie method needs to be coupled to the time stepping of a reaction-diffusion equation using a hybrid method such as that given by Eq. (4.10).

The three-dimensional simulation tool permitted investigation of the interior Ca^{2+} distribution of clustered channels by taking into account the spatial separation of channels (Rüdiger et al. 2010a, b; Rückl et al. 2015). Previous publications had assumed all the channels of a cluster form a shared disk-shaped source area without allowing passive space between the channels. It was found that Ca^{2+} distributions around open channels are non-homogeneous at the scale of a cluster for realistic channel distances. This leads to a separation of Ca^{2+} scale into a large self-coupling value (concentration at the channel pore of an open channel), and the much smaller cluster domain values, defined as an appropriate average Ca^{2+} concentration at closed channels while others are open. It is then clear that incorporating spatial separation (as opposed to a tight cluster model) leads to models which allow a much better description of experimentally observed puffs see Sect. 4.3.2.

4.3.5 Simulations with Discrete Ca^{2+} Ions

The modeling approaches described above recognized the importance of number fluctuations in the binding to the channels and formulated hybrid models where the deterministic Ca^{2+} concentration is coupled to stochastic channel binding models (Rüdiger et al. 2007). More recently, however, it was found that local fluctuations stemming from diffusive noise of Ca^{2+} ions may also have a crucial influence in Ca^{2+} dynamics. Diffusive noise of Ca^{2+} regards the fluctuating number of ions that are in the neighborhood of the receptors and are available for binding to them. This noise source is similar to the noise in the diffusion of a chemoattractant that was considered in the classic work of Berg and Purcell (Berg and Purcell 1977).

A straightforward method to take diffusive noise into account involves tracking the exact diffusive paths of each individual ion in the computational domain. Doing so in the complete domain is computationally very intensive and, therefore, Flegg et al. applied spatial stochastic multiscale modeling in order to accurately incorporate diffusive noise (Flegg et al. 2013). In the two-regime method (Flegg et al. 2011), Brownian trajectories of the particles and binding events are followed in a small space surrounding the receptor cluster, while further away from the cluster the fluctuating numbers of ions in larger three-dimensional compartments are calculated. This method saves a considerable amount of simulation time while not compromising the microscopic detail needed for the binding dynamics close to the receptors. Flegg et al. showed that this approach can be used to calculate interpuff intervals for a cluster of nine channels.

A compartment-based approach was also used in the simulation of Wieder et al. (2015). There the influence of fluctuations in Ca^{2+} ion number on the equilibrium behavior of a single channel was studied and it was found that those fluctuations increase the open probability compared to the standard deterministic model. In an investigation of fluctuations in the number of Ca^{2+} ions in a single compartment in contact with the bulk, Weinberg and Smith found that mobile Ca^{2+} buffers may increase the size of fluctuations of $[Ca^{2+}]$ around its equilibrium value

(Weinberg and Smith 2014). Together, these studies hint at the presence of discrete Ca^{2+} noise, but further research is needed to draw clear conclusions regarding their relevance to Ca^{2+} release models.

4.4 Stochastic Intracellular Ca^{2+} Signals

Global synchronization of release results in cell-wide oscillations or waves (Berridge 1990; Lechleiter et al. 1991; Camacho and Lechleiter 1993) that can last up to several tens of seconds. Despite the ubiquity of Ca^{2+} oscillations in many cell types and many years of experimental and modeling research, there is still no consensus on the basic mechanism of the regenerative discharges. Here we would like to briefly look at the most widely discussed models and a few aspects in computational modeling that have been in focus recently. For a thorough discussion of the possible physiological mechanisms, we refer readers to the excellent review by Dupont et al. (2011).

Models of Ca^{2+} oscillations, just as any other kind of oscillation in biology, including cell cycle and circadian rhythms, rely on a number of nonlinear feedback processes (Nov'ak and Tyson 2008). Limiting the present discussion to intracellular IP_3-controlled oscillations, two groups of mechanisms have been put forward. One group is based on the observation that IP_3R is biphasically regulated by Ca^{2+}. In its essence, oscillations are obtained by an alternation of activating and inhibiting binding to the receptor, which is obtained by various channel gating schemes such as for instance the DeYoung-Keizer scheme. This way, the global oscillations build on the same processes as the local signals discussed above and this suggests viewing the global signals as synchronized local signals. However, the times between the Ca^{2+} puffs are much shorter than those of the Ca^{2+} oscillations. In particular, recovery of the receptor from inhibition takes a few seconds at most, whereas oscillation periods can be longer than one minute. This and the very different durations of puffs and waves point to a shortcoming of this family of models.

A further group of models take into account the fact that in many cell types the concentration of IP_3 is also variable and may therefore drive Ca^{2+} oscillations. Several possibilities have been proposed including stimulation of IP_3 synthesis by released Ca^{2+} (Meyer and Stryer 1988) and Ca^{2+}-activated down-regulation of G-protein-coupled IP_3 production (Cuthbertson and Chay 1991). Other studies featured passive IP_3 variability (Dupont and Erneux 1997) or included several types of the mentioned mechanisms to allow a detailed quantitative comparison (De Pitt'a et al. 2009).

More recently a detailed study of release from a receptor cluster has been used to explain the dichotomy of puffs and waves observed in many cell types including *Xenopus* oocytes. Rückl et al. analyzed the modified DeYoung-Keizer model previously used to study the Ca^{2+} puffs and found that it is capable of producing both short-lived release as well as wave-like release that lasts for several seconds (Rückl et al. 2015). In the model, long-lasting events are accompanied by unbinding of IP_3

from the receptor. Since these long events have a much larger total Ca^{2+} release, they are more likely to stimulate neighboring clusters and thus tend to synchronize release as observed during a wave. Since the large events are less frequent than the short events, the model produces periods of global events in the order of the experimentally observed inter-spike intervals. Interestingly, the unbinding of IP_3 occurs with a short delay compared to the peak position, resulting in a delayed peak of free IP_3 concentration that has also been observed experimentally (Tanimura et al. 2009; Gaspers et al. 2014).

The mechanisms described above can in principle be used within a deterministic differential equation model. This has frequently been done to analyze whole-cell oscillations. However, with the increasing spatial resolution and characterization of local Ca^{2+} release in experiments, the role of noise in the appearance and generation of global Ca^{2+} signals has been recognized. This has prompted a way of modeling in accord with noise-driven, excitable local release, which thus shares similarities to the behavior found in the propagation of neuronal action potentials.

A number of experimental studies characterized puffs as the basic building blocks of global signals (Parker et al. 1996; Smith and Parker 2009). Since puffs are noise-driven as discussed above, Falcke and co-workers postulated that their inherent randomness carries over to waves (Skupin et al. 2010). According to this picture, a random opening of channels in one or several clusters triggers the activation of adjacent clusters, thus facilitating the spreading of a wave through the cell. These ideas also provide an explanation of the inherent randomness of Ca^{2+} oscillations, which is apparent most clearly in their fluctuating inter-spike period.

Besides the duration of an event, stochastic modeling addresses the different inter-puff times (a few seconds) and inter-wave times (several tens of seconds to minutes). In the approach by Falcke and co-workers the long periods of global oscillations are created by the waiting time for a sufficiently large local event encompassing several clusters (a nucleation event) (Thurley and Falcke 2011). Alternatively, it has also been suggested that the amplitude of elementary release events is distributed randomly. Accordingly, only the largest events would have sufficient potency to spread to adjacent clusters (Rückl et al. 2015). The latter model also explains why a cluster stays refractory after a wave for several seconds while it admits puffs shortly after termination of a prior puff (Marchant and Parker 2001).

4.5 Outlook of Intercellular Ca^{2+} Waves with Stochastic IP_3R Dynamics

Intercellular Ca^{2+} waves (ICWs) can be induced in response to bath application of glutamate or ATP in glial cells. Mechanical or electrical stimulation can also generate ICWs. Experimental data showed that the permeability of intracellular IP_3 messenger or Ca^{2+} ions through gap junctions and the spreading of extracellular ATP messengers are important mechanisms for ICWs.

Currently, many simulation models discussed for ICWs are based on deterministic signal dynamics. The biologically realistic features, such as the clustering distribution of IP_3R and the stochastic channel dynamics have been paid less attention. It has been found that the application of stochastic methods is necessary and useful to describe intracellular Ca^{2+} signaling. In this chapter we have presented how various theoretical concepts such as Markov chains, the Gillespie algorithm, the Langevin approach and hybrid modeling can be applied to the study of intracellular Ca^{2+} dynamics. Thus it is necessary to discuss the intercellular Ca^{2+} waves with stochastic dynamics of clustered IP_3R channels.

One can expect that the stochastic dynamics of clustered IP_3R channels can affect not only the intracellular Ca^{2+} signals, but also the intercellular Ca^{2+} waves. The ICWs model with stochastic and clustered IP_3R channels will be considerably closer to experimental observations and provide more quantitative insights into ICWs. For the coupled glial cells, it raises the model's complexity by integration of grouped-cell processes which span many scales, from single IP_3R channel dynamics and clustered channels, to intracellular cells and intercellular cells. Thus, a challenge is to develop an ICW model which is complex enough to account for the stochastic and clustered IP_3R channel dynamics, and at the same time is simple enough to be computationally efficient for numerical modeling. We believe that such an ICW model can lead to a deeper understanding of the ICW mechanisms of glial cells.

Acknowledgements Shuai acknowledges support from the China National Funds for Distinguished Young Scholars under grant 11125419, the National Natural Science Foundation of China under grants 31370830 and 11675134, and the Fujian Province Funds for Leading Scientist in Universities. S.R. acknowledges support from the Deutsche Forschungsgemeinschaft (RU 1660 and IRTG 1740).

References

Alfonsi A, Cances E, Turinici G, Di Ventura B, Huisinga W (2005) Exact simulation of hybrid stochastic and deterministic models for biochemical systems. ESAIM: Proc 14:1–13

Berg HC, Purcell EM (1977) Physics of chemoreception. Biophys J 20(2):193–219

Berridge MJ (1990) Calcium oscillations. J Biol Chem 265(17):9583–9586

Berridge MJ, Bootman MD, Roderick HL et al (2003) Calcium signalling: dynamics, homeostasis and remodelling. Nat Rev Mol Cell Biol 4:517–529

Camacho P, Lechleiter JD (1993) Increased frequency of calcium waves in Xenopus laevis oocytes that express a calcium-ATPase. Science 260:226–229

Cao P, Donovan G, Falcke M, Sneyd J (2013) A stochastic model of calcium puffs based on single-channel data. Biophys J 105(5):1133–1142

Cuthbertson KSR, Chay TR (1991) Modelling receptor-controlled intracellular calcium oscillators. Cell Calcium 12(2):97–109

De Pitt'a M, Goldberg M, Volman V, Berry H, Ben-Jacob E (2009) Glutamate regulation of calcium and $I\,P_3$ oscillating and pulsating dynamics in astrocytes. J Biol Phys 35(4):383–411

DeRemigio H, Groff JR, Smith GD (2008) Calcium release site ultrastructure and the dynamics of puffs and sparks. Math Med Biol 25(1):65. ISSN 1477–8599

DeYoung G, Keizer J (1992) A single-pool inositol 1,4,5-trisphosphate-receptor-based model for agonist-stimulated oscillations in Ca^{2+} concentration. Proc Nat Acad Sci USA 89:9895–9899
Di Capite J, Ng SW, Parekh AB (2009) Decoding of cytoplasmic Ca^{2+}+ oscillations through the spatial signature drives gene expression. Current Biol 19(10):853–858. ISSN 0960-9822
Dolmetsch RE, Xu K, Lewis RS (1998) Calcium oscillations increase the efficiency and specificity of gene expression. Nature 392:933–936
Dupont G, Combettes L, Bird GS, Putney JW (2011) Calcium oscillations. Cold Spring Harb Perspect Biol 3(3)
Dupont G, Erneux C (1997) Simulations of the effect of inositol 1,4,5-trisphosphate 3-kinase and 5-phosphatase on Ca^{2+} oscillations. Cell Calcium 22:321–331
Falcke M (2003) On the role of stochastic channel behavior in intracellular Ca^{2+} dynamics. Biophys J 84(1):42–56
Falcke M (2004) Reading the patterns in living cells-the Physics of Ca^{2+} signaling. Adv Phys 53(3):255–440
Flegg MB, Chapman SJ, Erban R (2011) The two-regime method for optimizing stochastic reaction–diffusion simulations. J Royal Soc Interface, rsif20110574
Flegg M, Ruediger S, Erban R (2013) Diffusive spatio-temporal noise in a first-passage time model for intracellular calcium release. J Chem Phys 138:154103
Fox RF (1997) Stochastic versions of the Hodgkin-Huxley equations. Biophysial J 72:2068–2074
Fox RF, Lu Y (1994) Emergent collective behavior in large numbers of globally coupled independently stochastic ion channels. Phys Rev E 49(4):3421–3431
Gaspers LD, Bartlett PJ, Politi A, Burnett P, Metzger W, Johnston J, Joseph SK, Hofer T, Thomas AP (2014) Hormone-induced calcium oscillations depend on cross-coupling with inositol 1, 4, 5-trisphosphate oscillations. Cell Rep 9(4):1209–1218
Gillespie DT (1976) A general method for numerically simulating the stochastic time evolution of coupled chemical reactions. J Comput Phys 22:403–434
Gillespie DT (1977) Exact stochastic simulation of coupled chemical reactions. J Phys Chem 81:2340–2361
Gibson MA, Bruck J (2000) Efficient exact stochastic simulation of chemical systems with many species and many channels. J Phys Chem A 104(9):1876–1889
Hodgkin AL, Huxley AF (1952) A quantitative description of membrane current and its application to conduction and excitation in nerve. J Phys 117(4):500
Huang YD, Rüdiger S, Shuai JW (2011) Modified Langevin approach for a stochastic calcium puff model. Eur Phys J B 83:401–407
Huang YD, Ruediger S, Shuai JW (2013) Channel-based Langevin approach for the stochastic Hodgkin-Huxley neuron. Phys Rev E 87:012716
Johenning FW, Theis A-K, Pannasch U, Rückl M, Rüdiger S, Schmitz D (2015) Ryanodine receptor activation induces long-term plasticity of spine calcium dynamics. PLoS Biol 13(6):e1002181
Lechleiter JD, Girard S, Peralta E, Clapham D (1991) Spiral calcium wave propagation and annihilation in Xenopus laevis oocytes. Science 252:123–126
Li Y, Rinzel J (1994) Equations for insp3 receptor-mediated [Ca^{2+}] oscillations derived from a detailed kinetic model: a hodgkin-huxley like formalism. J Theoret Biol 166:461–473
Lytton J, Westlin M, Burk SE, Shull GE, MacLennan DH (1992) Functional comparisons between isoforms of the sarcoplasmic or endoplasmic reticulum family of calcium pumps. J Biol Chem 267(20):14483–14489
Neher E (1998) Vesicle pools and Ca^{2+} microdomains: New tools for understanding their roles in neurotransmitter release. Neuron 20:389–399
Nov'ak B, Tyson JJ (2008) Design principles of biochemical oscillators. Nat Rev Mo Cell Biol 9(12):981–991
Marchant JS, Parker I (2001) Role of elementary Ca^{2+} puffs in generating repetitive Ca^{2+} oscillations. EMBO J 20:65–76
Meyer T, Stryer L (1988) Molecular model for receptor-stimulated calcium spiking. Proc Nat Acad Sci 85(14):5051–5055

Orio P, Soudry D (2012) Simple, fast and accurate implementation of the diffusion approximation algorithm for stochastic ion channels with multiple states. PLoS One 7:e36670
Parker I, Yao Y (1996) Ca^{2+} transients associated with openings of inositol trisphosphate-gated channels in Xenopus oocytes. J Physiol (Lond) 491:663–668
Parker I, Choi J, Yao Y (1996) Elementary events of $InsP_3$-induced Ca^{2+} liberation in Xenopus oocytes: hot spots, puffs and blips. Cell Calcium 20(2):105–121
Qi H, Li LX, Shuai JW (2015) Optimal microdomain corsstalk between endoplasmic reticulum and mitochondria for Ca2+ oscillations. Sci Rep 5:7984, 1–11
Roberts WM (1994) Localization of calcium signals by a mobile calcium buffer in frog saccular hair cells. J Neurosci 14(5):3246–3262
Rüdiger S, Shuai JW, Huisinga W, Nagaiah Ch, Warnecke G, Parker I, Falcke M (2007) Hybrid stochastic and deterministic simulations of calcium blips. Biophys J 93:1847–1857
Rüdiger S, Shuai JW, Sokolov IM (2010a) Law of mass action, detailed balance, and the modeling of calcium puffs. Phys Rev Lett 105:048103
Rüdiger S, Nagaiah Ch, Warnecke G, Shuai JW (2010b) Calcium Domains around Single and Clustered IP_3 Receptors and Their Modulation by Buffers. Biophys J 99(1):3–12
Rüdiger S (2014a) Stochastic models of intracellular calcium signals. Phys Rep 534(2):39–87
Rüdiger S (2014b) Excitability in a stochastic differential equation model for calcium puffs. Phys Rev E 89(6):062717
Rüdiger S, Qi H, Huang Y, Shuai J (2014) Frequency and relative prevalence of calcium blips and puffs in a model of small ip3r clusters. Biophysical Journal 106:2353–2363
Rückl M, Parker I, Marchant JS, Nagaiah C, Johenning FW, Rüdiger S (2015) Modulation of elementary calcium release mediates a transition from puffs to waves in an ip3r cluster model. PLoS Comput Biol 11(1):e1003965
Rusakov DA (2015) Disentangling calcium-driven astrocyte physiology. Nat Rev Neurosci 16(4):226–233
Shuai JW, Jung P (2002) Stochastic properties of Ca^{2+} release of inositol 1, 4, 5-trisphosphate receptor clusters. Biophys J 83:87–97
Shuai JW, Jung P (2003) Langevin modeling of intracellular calcium dynamics. Understanding Calcium, Dynamics, pp 231–252
Skupin A, Kettenmann H, Falcke M (2010) Calcium signals driven by single channel noise. PLoS Comput Biol 6(8):1183–1186. ISSN 1553-734X
Smith GD (1996) Analytical steady-state solution to the rapid buffering approximation near an open Ca2+ channel. Biophys J 71:3064–3072
Smith IF, Parker I (2009) Imaging the quantal substructure of single IP3R channel activity during Ca2+ puffs in intact mammalian cells. Proc Natl Acad Sci USA 106(15):6404
Smith IF, Wiltgen SM, Shuai J, Parker I (2009) Ca2+ puffs originate from pre-established stable clusters of inositol trisphosphate receptors. Sci Signaling 2(98):ra77
Tanimura A, Morita T, Nezu A, Shitara A, Hashimoto N, Tojyo Y (2009) Use of fluorescence resonance energy transfer-based biosensors for the quantitative analysis of inositol 1, 4, 5-trisphosphate dynamics in calcium oscillations. J Biol Chem 284(13):8910
Thurley K, Falcke M (2011) Derivation of Ca^{2+} signals from puff properties reveals that pathway function is robust against cell variability but sensitive for control. Proc Natl Acad Sci USA 108(1):427
Ullah G, Parker I, Mak DOD, Pearson JE (2012) Multi-scale data-driven modeling and observation of calcium puffs. Cell Calcium 52:152
Volterra A, Liaudet N, Savtchouk I (2014) Astrocyte Ca^{2+} signalling: an unexpected complexity. Nat Rev Neurosci 15(5):327–335
Weinberg SH, Smith GD (2014) The influence of Ca^{2+} buffers on free $[Ca^{2+}]$ fluctuations and the effective volume of Ca^{2+} microdomains. Biophys J 106(12):2693–2709
Wieder N, Fink R, von Wegner F (2015) Exact stochastic simulation of a calcium microdomain reveals the impact of Ca^{2+} fluctuations on ip3r gating. Biophys J 108(3):557–567